are expanded the vapor gas from liquid water.

(3) The expanded vapor gas pushes away the flesh air (oxygen gas) gas by the vaporization force insted of the entraiment air into the heat source by drag force.

(4) The expanded vapor gas also blow out the flame, and push away from the vaporizing fuel gas from heat source by heat flux. The mechanism of the extinguishing oil fire by fine water mist is almost similar by gas agent. The water mist is a kind of the suffocation extinguishing agent.

Above reasons, the efficiency of the extinguishing fire by using the water mist suppression system increases in the enclosure compartment fire, because of the suffocation effect. Furthermore the mechanism of the extinguishing oil fire by the fine water mist also has a cooling effect by vaporizing water as like as sprinkler. However the cooling effect needs that the sprayed out fine mist droplets must be penetrated into the fire flame directly and/or be reached on the fire fuel gas surface directly. the momentum energy of the sprayed out fine water mist flow might need to defeat the drag force of the fire flame.

Co Formation Characteristics of Methane-Air Diffusion Flames Doped with Halon Replacements

YUKO SASO
National Research Institute of Fire and Disaster
14 1 Nakahara 3-chome, Mitaka, Tokyo 181-8633, Japan

MAKIHITO NISHIOKA
Institute of Engineering Mechanics and Systems, University of Tsukuba
Tsukuba, Ibaraki 305-8573, Japan

TADAO TAKENO
Department of Mechanical Engineering, Nagoya University
Chikusa-ku, Nagoya 464-8601, Japan

ABSTRACT

To explore the potential risk of increased CO with halon replacements in fires, methane-air diffusion flames doped with suppressants were studied numerically. The suppressants investigated are nitrogen, HFC-23 and HFC-227ea, as well as Halon 1301. When Halon 1301 is doped in the air side of the counterflow diffusion flame at constant oxidizer and fuel flow velocities, little change is observed in the production rate of CO. An addition of nitrogen causes reduced CO production because of decreased fuel consumption, while an addition of HFC-227ea causes a significant increase in both the maximum CO mole fraction and its production rate. CO in the HFC-227ea-doped diffusion flames is formed in two different regions, the methane oxidation region and an additional region on the oxidizer side of the flame, in which CO is produced via the oxidation of the suppressant. When normalized by the total amount of carbon released in the flame, the CO production rate is almost constant with variations of suppressant and its concentration. The increased CO production with HFC-227ea is attributed to the excess supply of carbon into the flame.

KEYWORDS: carbon monoxide, combustion modelling, halogenated suppressant, halon 1301, halon replacement, inhibitor, inhibition, fire suppression, extinction.

INTRODUCTION

Following the ban of halon production to protect the stratospheric ozone layer, several replacements have come into wide use in total-flooding fire extinguishing systems. These

replacements include fluorinated hydrocarbons (HFCs) and inert gases such as nitrogen. They are, however, less effective than halons and require higher agent concentrations to extinguish a fire. Furthermore, HFCs cause excessive production of toxic hydrogen fluoride (HF) in fire. Extensive research has focused on evaluation of potential risk of HF production by HFCs [1, 2]. On the other hand, carbon monoxide (CO) formation during fire suppression using halon replacements has yet to be addressed.

The formation of CO in enclosure fires is known to be the leading cause of fire deaths [3]. While it is suggested that CO formation in fires is controlled by reaction kinetics [3], detailed chemical kinetics of oxidation of HFCs has not been fully established yet. Detailed chemical kinetic and thermodynamic information for C_1- and C_2-HFCs was developed at the National Institute of Standards and Technology (NIST) [4]. Subsequently, Hynes et al. [5] developed an oxidation kinetic model of HFC-227ea (C_3HF_7), which is used as a halon replacement chemical. Using the model of Hynes et al., Moghtaderi et al. [6] predicted the formation of toxic compounds in enclosure fires during suppression, and suggested that enclosure fires with and without fire suppressants behave differently in terms of the CO production. Moore and Yamada [7] also suggested that the concentration of CO would increase when nitrogen gas is discharged into a fire.

To explore the potential risk of increased CO production in fires suppressed by halon replacement, numerical simulations were performed for methane-air counterflow diffusion flames doped with gaseous fire suppressants with detailed chemistry and transport [8]. The results showed that HFC-227ea causes a significant increase in CO production through the oxidation of the agent. This prediction is supported by recent full-scale fire suppression experiments by Su and Kim [9], who also attributed the increased CO production to agent-flame interaction.

The present paper is an extension of preliminary work reported in Ref. 8. Recently L'EspÈrance et al. [10] and Williams et al. [11] performed refinement of the NIST HFC kinetic model [4] and of Hynes' HFC-227ea oxidation mechanism [5], based on their experimental data on intermediate species concentration profiles in low-pressure flat flames, and on the laminar burning velocity data of Linteris et al. [12]. The present study employs this refined model, which can better predict the experimentally observed characteristics of HFC-227ea-doped flames. In this paper, methane-air counterflow diffusion flames doped with nitrogen, HFC-23 (CHF_3), HFC-227ea and halon 1301 (CF_3Br) are studied numerically. When Halon 1301 is doped in the air side of the counterflow diffusion flame at constant oxidizer and fuel flow velocities, little change is observed in the production rate of CO. Addition of nitrogen reduces CO production because of decreased fuel consumption, while HFC-227ea causes a significant increase in both the maximum CO mole fraction and its production rate. It is found that CO in the HFC-227ea-doped diffusion flames is formed in two different regions, the methane oxidation region and an additional region on the oxidizer side of the flame, in which CO is produced via the oxidation of the suppressant. The CO production characteristics are evaluated quantitatively in terms of the emission index.

NUMERICAL CALCULATIONS

The kinetic model employed in the present study is composed of three parts: GRI-Mech 2.11 [13] for methane oxidation with nitrogen chemistry deleted (31 species and 175 reactions); the HFC oxidation mechanism taken from Ref. 11 which is based on the NIST HFC model [4] and the work of Hynes et al. [5] with the refinement by Saso et al.[14] and L'EspÈrance et al. [10]

(60 species and 633 reactions); and the Br chemistry taken from the work of Babushok et al. [15] (10 species and 89 reactions). The thermochemical data were taken from the GRI-Mech [13] for the C–H–O species and from Refs. 11 and 15 for the F and Br-containing species, respectively.

Figure 1 shows the schematic illustration of the axisymmetric steady counterflow flat diffusion flame stabilized between the two opposed nozzles. The mathematical model and the governing equations follow that of Kee et al. [16] and Dixon-Lewis [17]. The numerical scheme is essentially that developed by Kee et al. for the one-dimensional premixed flame [18], and was modified for the calculation of the counterflow flame by Nishioka et al. [19]. Thermochemical and transport properties were calculated with CHEMKIN II [20] and the transport subroutine package of Ref. 21, respectively. Computations were performed for atmospheric pressure flames with an unburnt gas temperature of 298 K, employing central differencing for the convective terms and adaptive gridding with the total number of grid points between 150-230. The distance between the nozzles is fixed at 1.5 cm. At the nozzle exit the radial component of the flow velocity is set equal to zero, while the axial components of the opposed flow velocities u are kept equal and are fixed at 40 cm/s.

To calculate extinction concentrations of suppressants, extinction curves were generated as a function of the suppressant concentration at a constant flow velocity, employing the flame-controlling continuation method developed by Nishioka et al. [22] with a boundary condition modified to obtain the critical concentration of suppressant instead of the extinction strain rate used in Ref. 22. Examples of the calculated extinction curves are presented in Ref. 23.
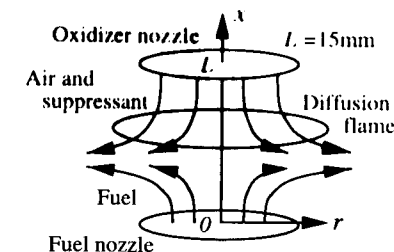
FIGURE 1. Schematic illustration of the counterflow diffusion flame model.

RESULTS AND DISCUSSION

Structural Change of Counterflow Diffusion Flame with Suppressant Doping

Figure 2 presents the temperature and major species profiles in the methane-air counterflow diffusion flames with and without suppressant (nitrogen or halon 1301) at the oxidizer side, computed with the fuel and the oxidizer boundary velocities of 40 cm/s. In Fig. 2, the left end of the horizontal axis corresponds to the exit of the fuel nozzle, and the right end corresponds to that of the oxidizer nozzle. It is seen that addition of nitrogen causes a significant reduction of flame temperature along with a decrease in the peak CO_2, CO, and H_2O mole fractions, while halon 1301 causes almost no change in the flame temperature or the peak CO_2 and CO mole fractions.

Figure 3 presents the temperature and major species profiles for HFC-23 and HFC-227ea. In Fig. 3(a), a moderate reduction of the flame temperature is observed and little change in the peak CO_2 and CO mole fractions when HFC-23 is added to the flame. On the other hand, in Fig. 3(b) where HFC-227ea is the inhibitor, a significant increase in the peak CO mole fraction is observed. Also observed in Figs. 3(a) and 3(b) are an enormous amount of HF produced along with a commensurate reduction in H_2O due to the effect of the suppressants.

Because CO is an intermediate species as well as a final product in methane combustion, the
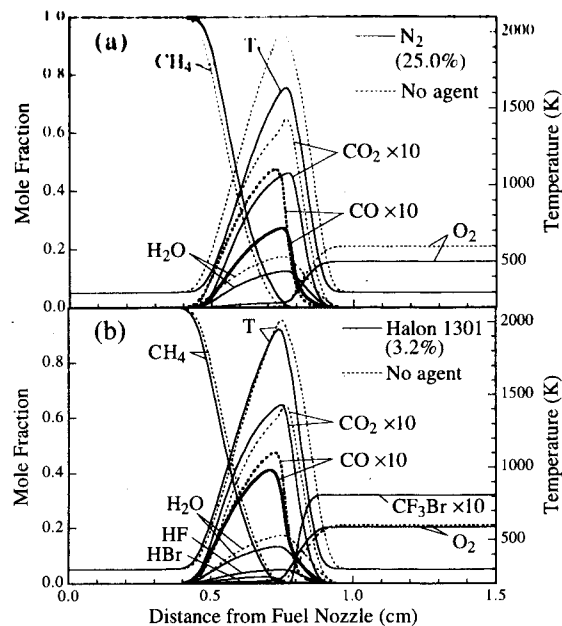
FIGURE 2. Computed temperature (T) and major species profiles in methane-air counterflow diffusion flames doped with (a) 0% and 25.0% nitrogen and (b) 0% and 3.2% halon 1301. The conditions with the suppressants are near extinction. Computations were performed at a constant fuel and oxidizer boundary velocity of 40 cm/s.
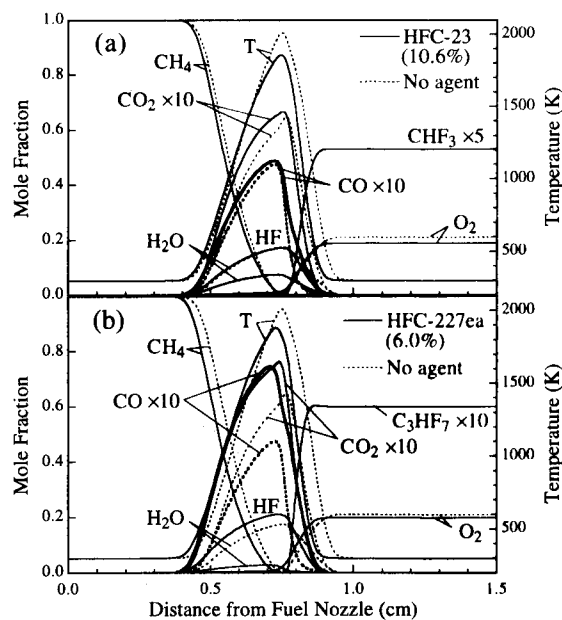
FIGURE 3. Computed temperature (T) and major species profiles in methane-air counterflow diffusion flames doped with (a) 0% and 10.6% HFC-23 and (b) 0% and 6.0% HFC-227ea. The conditions with the suppressants are near extinction. Computations were performed at a constant fuel and oxidizer boundary velocity of 40 cm/s.

peak CO mole fraction in the flame does not directly represent the amount of CO produced. In order to analyze the CO formation and consumption process in the flame, we performed reaction flux analyses. Figure 4 presents the rate profiles of major CO generation and consumption reactions as well as the profile of total CO production rate, computed for (a) the uninhibited flame, (b) the nitrogen- and (c) halon 1301-doped flames shown in Fig. 2. When no agent is added, the main CO formation and consumption pathways in the counterflow diffusion flame are

$$HCO + M \rightarrow H + CO + M \tag{R1}$$

$$CO + OH \rightarrow H + CO_2 \tag{R2}$$
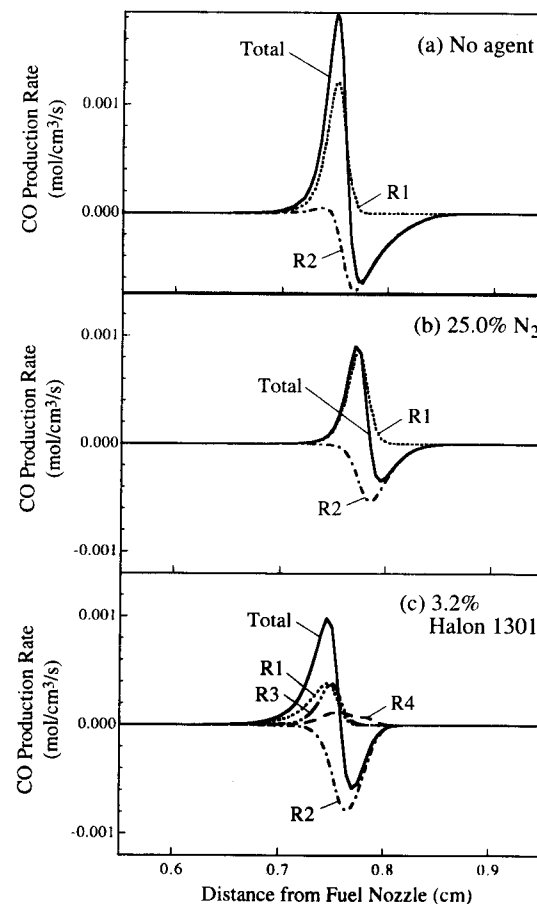
FIGURE 4. Rate profiles of major CO generation and consumption reactions and the total CO production. The conditions are the same as those of Fig. 2.

where M is a third body for collision. Reaction (R1) shows its maximum rate in the methane oxidation region in the flame. CO produced there is transported through diffusion toward the oxidizer side of the flame where reaction (R2) becomes significant.

In the nitrogen- and halon 1301-doped flames, the main pathway for the CO formation and consumption is also reactions (R1) and (R2) as seen in Figs. 4(b) and 4(c). In the halon 1301-doped flame, however, a new reaction for CO formation appears:

$$Br + HCO \rightarrow HBr + CO \tag{R3}$$

With a large doping of halon 1301 near extinction, the flux of R3 approaches that of R1. Reaction (R3) has its maximum rate near the location of the peak of reaction (R1), and compete with R1 to produce CO from HCO, which is generated through the oxidation of methane.

Figure 5 presents the rate profiles of major CO generation and consumption reactions as well as that of total CO production, computed for the HFC-23- and HFC-227ea-doped flames shown in Fig. 3. When HFC-23 is added (Fig. 5(a)), an entirely different pathway for CO formation appears:

$$CFO + M \rightarrow CO + F + M \tag{R4}$$
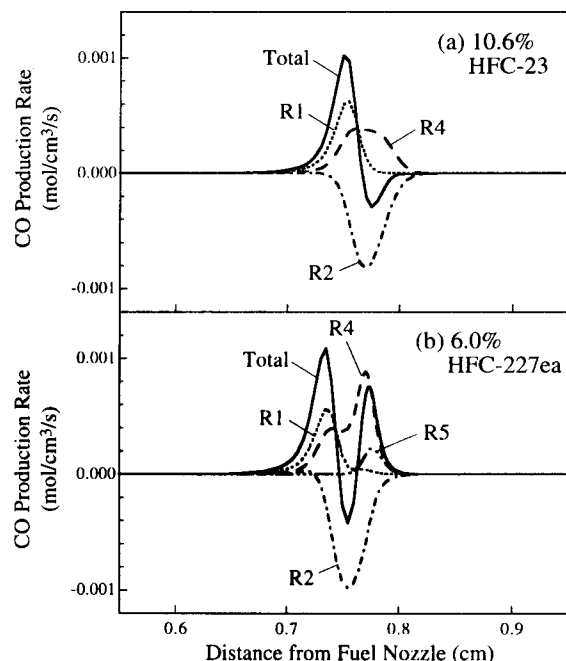
FIGURE 5. Rate profiles of major CO generation and consumption reactions and the total CO production. The conditions are the same as those of Fig. 3.

CFO in reaction (R4) is produced through the oxidation of the agent. Reaction (R4) has its maximum rate near the location of the peak of reaction (R2), and cancels out the negative peak of the total CO production rate profile as seen in Fig. 5(a). Particularly near the extinction concentration, reaction (R4) becomes the dominant pathway for CO formation. In Fig. 5(b), where HFC-227ea is used, reaction (R4) is again the dominant pathway for CO formation. In addition, the following reaction contributes significantly to CO production:

$$CF_3CO \rightarrow CF_3 + CO \tag{R5}$$
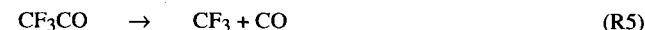
As a result, the total CO production rate in Fig. 5(b) shows a unique M-shaped profile, demonstrating that CO in the HFC-227ea-doped diffusion flame is formed in two different regions, the methane oxidation region through R1 and an additional region on the oxidizer side where CO is produced via the oxidation of the agent through R4 and R5.

CO Emission Index of Counterflow Diffusion Flame

We next evaluate quantitatively the CO production characteristics of the counterflow diffusion flame in terms of the emission index (EI). EI was first introduced by Takeno et al. [24] for the purpose of evaluating the NO emission characteristics [19]. It was defined as

$$EI_{NO} = \frac{\int_O^L W_{NO} \dot{\omega}_{NO} dx}{-\int_O^L W_F \dot{\omega}_F dx} \tag{Eq. 1}$$

where O and L denote the boundaries of the computational domain, $\dot{\omega}_{NO}$ and $\dot{\omega}_F$ the mole production rate, and W_{NO} and W_F the molecular weight of NO and fuel, respectively. While the EI of Eq. 1 represents the mass production rate of NO per unit fuel mass consumption rate, the present study employs the following definition of EI for the CO production on a molar basis, in order to compare the number of carbon atoms released from the fuel and number of CO molecules produced. That is,

$$\Omega_k = \int_O^L \dot{\omega}_k dx \tag{Eq. 2}$$

$$EI_{CO} = \frac{\Omega_{CO}}{-\Omega_{CH_4}} \tag{Eq. 3}$$

Here k denotes any species.

Figure 6 presents (a) the integrated CO production rate (Ω_{CO}) computed with Eq. 2 by integrating the total CO production rate profile of Figs. 4 and 5, and (b) EI_{CO} computed with Eq. 3, as a function of the suppressant concentration at the oxidizer boundary normalized with the computed critical concentration for extinction of each suppressant (nitrogen: 25.2%, halon 1301: 3.22%, HFC-23: 10.73%, HFC-227ea: 6.07%). In Fig. 6(a), it is found that Ω_{CO} is decreased with nitrogen doping, while it is unchanged with halon 1301 or HFC-23 doping, and is increased with HFC-227ea doping. In Fig. 6(b), it is found that EI_{CO} is kept constant at approximately 0.3 when nitrogen or halon 1301 is doped, while it is remarkably increased with addition of HFC-23 and HFC-227ea. The constant EI_{CO} with addition of nitrogen demonstrates a reduced methane consumption proportional to the reduction in CO production. It is also seen that EI_{CO} exceeds unity with an addition of HFC-227ea near extinction, indicating that CO must be produced partly from the agent.

If we define the index in terms of the total carbon released not only from the fuel but also the

agent, we have

$$EI_{CO}^{*} = \frac{\Omega_{CO}}{-\Omega_{CH_4} - \Omega_{CF_3Br} - \Omega_{CHF_3} - 3\Omega_{C_3HF_7}} \qquad (Eq.\ 4)$$

Fig. 6(c) presents EI_{CO}^{*} as a function of the normalized suppressant concentration. It is seen that EI_{CO}^{*} is almost constant for all suppressants over the concentration ranges investigated in the present study. Therefore the increased CO production rate with HFC doping can be attributed mainly to the excess supply of carbon atoms into the flame. The results of Fig. 6(c) also demonstrate that approximately 30% of total carbon released in the flame is converted to CO, regardless of the suppressant.

FIGURE 6. Variations of (a) integrated CO production rate, (b) EI_{CO}, and (c) EI^{*}_{CO}, as a function of suppressant concentration added to air normalized by the computed extinction concentration of each suppressant. The fuel and oxidizer boundary velocities are 40 cm/s.

Also compared in Figs. 6(a)-(c) are the results computed with the HFC kinetic model of Ref. 5 (plotted with dashed lines, referred as Ref. 8) and that of Ref. 11 (solid lines, this work). Fig. 6 shows that no significant difference is observed in Ω_{CO}, EI_{CO}, and EI_{CO}^{*} between the two models, although the critical concentration for extinction was found to be moderately different between the model of Ref. 5 (5.84%) and that of Ref. 11 (6.07%).

Figure 7 presents the dominant reaction pathways for oxidation of HFC-227ea in the methane-air counterflow diffusion flame doped with 6.0% of HFC-227ea at the oxidizer boundary, that were obtained by integrating each consumption reaction rate throughout the computational domain, employing the kinetic model of Ref. 11. This is the first reaction pathway analysis of HFC-227ea oxidation in a counterflow diffusion flame. The predicted reaction pathways are considerably different from those of a low pressure premixed flame presented by Williams et al. [11]. In the diffusion flame, hydrogen abstraction accounts for 42% of HFC-227ea destruction, while it accounts for only about 5% of HFC-227ea destruction in Ref. 11. Instead, the C-C scission, the primary destruction mechanism for HFC-227ea, is reduced to 48%, while in the premixed flame it accounted for almost 90% of agent removal. The enhanced H atom abstraction in the diffusion flame (primarily by F atom) is attributed to the relative importance of F and O atoms in the HFC-227ea destruction region due to the lack of methane-originated species. As a result, subsequent reaction channels via $(CF_3)_2CO$, CF_3CFO, and CF_3CO become more important in the diffusion flame. Another remarkable difference from Ref. 11 is the removal pathway of $CHF=CF_2$. In the premixed flame, the removal of $CHF=CF_2$ was almost exclusively by the reaction with H to produce CH_2F and CF_2. In the present diffusion flame, the significance of F atom again alters the dominant reaction to produce CHF_2 and CF_2.

FIGURE 7. Dominant reaction pathways for oxidation of HFC-227ea in the methane-air counterflow diffusion flame doped with 6.0% of HFC-227ea at the oxidizer-side boundary, computed with the fuel and oxidizer boundary velocities of 40 cm/s.

SUMMARY

CO formation characteristics of methane-air counterflow diffusion flames doped with halon replacements were studied numerically. Addition of nitrogen caused a significant reduction of flame temperature with the decrease in peak CO_2, CO, and H_2O mole fractions, while addition of halon 1301 caused almost no change in the flame temperature or the peak CO_2 and CO mole fractions. When HFC-23 was added, a moderate reduction of the flame temperature was observed and little change in the peak CO_2 and CO mole fractions, while HFC-227ea caused a significant increase in the peak CO mole fraction. Flux analyses identified the dominant CO formation and consumption pathways that are affected by the suppressant doping. CO in the HFC-227ea-doped diffusion flame was formed in two different regions, the methane oxidation region and an additional region on the oxidizer side of the flame, in which CO was produced via the oxidation of the suppressant. When normalized by the total amount of carbon released in the flame, the CO production rate was almost constant with variations in the suppressants and their concentrations. The increased CO production with HFC-227ea was attributed to the excess supply of carbon into the flame. The present study suggests that while the primary risk caused by the decomposition of HFCs is HF and/or CF_2O, the formation of CO should also be considered.

REFERENCES

1. Miziolek, A.W. and Tsang, W. (Ed.), Halon Replacements, ACS Symposium Series No. 611, The American Chemical Society, Washington, D.C., 1995.
2. Proceedings of Halon Options Technical Working Conference, Albuquerque, NM, 1994, 1995 and 1996.
3. Pitts, W. M., *Prog. Energy Combust. Sci.*, **21**, 197-237 (1995).
4. Burgess, D.R.F., Jr., Zachariah, M., Tsang, W. and Westmoreland, P.R., *Prog. Energy Combust. Sci.*, **21**, 453-529 (1996).
5. Hynes, R. G., Mackie, J. C. and Masri, A. R., *Combust. Flame*, **113**, 554-565 (1998).
6. Moghtaderi, B.,Dlugogorski, B. Z. and Kennedy, E. M., 3rd Asia-Oceania Symposium on Fire Safety Science, Singapore, June 1998, pp.239-250.
7. Moore, T. A. and Yamada, N., Halon Options Technical Working Conference, Albuquerque, NM, 12-14 May 1998, pp.330-338.
8. Saso, Y., Tsuruda, T. and Saito, N., *Report of National Research Institute of Fire and Disaster*, **87**, 14-24 (1999).
9. Su, J. Z. and Kim, A. K., *Proceedings of the 6th International Symposium on Fire Safety Science*, in press (1999).
10. L' EspÈrance, D., Williams, B. A. and Fleming, J. W., *Combust. Flame*, **117**, 709-731 (1999).
11. Williams, B. A., L' EspÈrance, D. M. and Fleming, J. W., *Combust. Flame*, **120**, 160-172 (2000).
12. Linteris, G. T., Burgess, D. R. Jr., Babushok, V., Zachariah, M., Tsang, W. and Westmoreland, P., *Combust. Flame*, **113**, 164-180 (1998)
13. Bowman, C. T., Hanson, R. K., Gardiner, W. C., Lissianski, V., Frenklach, M., Goldenberg, M. and Smith, G. P., GRI Report GRI 97/0020, Gas Research Institute, Chicago, 1997. (http://www.ME.Berkeley.edu/gri mech/)
14. Saso, Y., Zhu, D. L., Wang, H., Law, C. K. and Saito, N., *Combust. Flame*, **114**, 457-468 (1998).
15. Babushok, V., Noto, T., Burgess, D. R. F., Hamins, A. and Tsang, W., *Combust. Flame*, **107**, 351-367 (1996).
16. Kee, R. J., Miller, J. A., Evans, G. H. and Dixon-Lewis, G., *22nd Symp.(Int.) on Comb.*, The Combustion Institute, Pittsburgh, 1988, pp.1479 1494
17. Dixon-Lewis, G., *23rd Symp.(Int.) on Comb.*, The Combustion Institute, Pittsburgh, 1990, pp.305-324.
18. Kee, R. J., Grcar, J. F., Smooke, M. D. and Miller, J. A., Sandia Report SAND 85-8240, Sandia National Laboratories, Albuquerque, NM, 1985.
19. Nishioka, M., Nakagawa, S., Ishikawa, Y. and Takeno, T., *Combust. Flame*, **98**, 127-138 (1994).
20. Kee, R. J., Rupley, F. M. and Miller, J. A., Sandia Report SAND 89-8009B, Sandia National Laboratories, Albuquerque, NM, 1989.
21. Kee, R. J., Warnatz, J. and Miller, J. A., Sandia Report SAND 83-8209, Sandia National Laboratories, Albuquerque, NM, 1983.
22. Nishioka, M., Law, C. K. and Takeno, T., *Combust. Flame*, **104**, 328-342 (1996).
23. Saso, Y. and Saito, N., *6th International Symposium on Fire Safety Science*, in press (1999).
24. Takeno, T. and Nishioka, M., *Combust. Flame*, **92**, 465-468 (1993).